BNL-67923

JOURNAL OF GEOPHYSICAL RESEARCH, VOL. 105, NO. D11, PAGES 14,701–14,717, JUNE 16, 2000

# A comparison of the aerosol thickness derived from ground-based and airborne measurements

Seiji Kato,[1,2] Michael H. Bergin,[3] Thomas P. Ackerman,[4] Thomas P. Charlock,[5] Eugene E. Clothiaux,[6] Richard A. Ferrare,[5] Rangasayi N. Halthore,[7] Nels Laulainen,[4] Gerald G. Mace,[8] Joseph Michalsky,[9] and David D. Turner[4]

**Abstract.** The extinction optical thickness of particles obtained from scattering and absorption coefficients measured by an airborne integrating nephelometer and particle soot absorption photometer, respectively, is compared with the aerosol optical thickness derived from a ground-based multifilter rotating shadowband radiometer, a Sun photometer, and a Raman lidar for 9 days. These 9 days are selected from intensive operation periods of the Atmospheric Radiation Measurement in April 1997, September 1997, and August 1998 at the southern Great Plains. For April 1997 and September 1997 cases the difference between the extinction optical thickness of particles estimated from vertical profiles and the extinction optical thickness of aerosol derived from the multifilter rotating shadowband radiometer is not significant. For August 1998 cases when the boundary layer relative humidity is higher than April 1997 and September 1997 cases, the extinction optical thickness of particles is 0.03 to 0.07 less than the extinction optical thickness of aerosol. The difference corresponds to 25% to 31% of the extinction optical thickness of aerosol. Based on these comparisons, the upper and lower limits of the single-scattering albedo of particles present in the lower part of troposphere are 0.97 and 0.84, respectively.

## 1. Introduction

The extinction optical thickness of the atmosphere can be computed by measuring the attenuation of direct solar radiation. The aerosol extinction optical thickness in selected wavelength regions by Sun photometry [e.g., *Shaw,* 1983] is the residual optical thickness after the molecular scattering optical thickness and the ozone and nitrogen dioxide absorption optical thicknesses are subtracted from the extinction optical thickness. Since there is no other absorber known to have large cross sections and high concentrations in the wavelength region coinciding with regions of large aerosol extinction cross sections, this appears to be a reasonable assumption. However, whether this residual optical thickness (aerosol optical thickness) is equal to the extinction optical thickness of particles needs to be examined. Such comparison is crucial to understand aerosol optical properties and radiative transfer under clear-sky conditions.

For this reason we compare the extinction optical thickness of particles estimated from vertical profiles of scattering and absorption coefficients measured by an airborne integrating nephelometer and particle soot absorption photometer with the aerosol extinction optical thickness derived from a ground-based multifilter rotating shadowband radiometer [*Harrison et al.,* 1994]. Since the former is estimated explicitly by measuring scattering and absorption by particles we consider that the extinction is by particles in this paper. The latter is defined as the aerosol extinction optical thickness in this paper because an aerosol is defined as a suspension of particles in a gas; an aerosol refers to the particles and gas [e.g., *Prospero et al.,* 1983].

[1]Center for Atmospheric Sciences, Hampton University, Hampton Virginia.

[2]Also at Atmospheric Sciences, NASA Langley Research Center, Hampton, Virginia.

[3]School of Civil and Environmental Engineering and School of Earth and Atmospheric Sciences, Georgia Institute of Technology, Atlanta.

[4]Pacific Northwest National Laboratory, Richland, Washington.

[5]Atmospheric Sciences, NASA Langley Research Center, Hampton, Virginia.

[6]Department of Meteorology, The Pennsylvania State University, University Park.

[7]Department of Applied Science, Brookhaven National Laboratory, Upton, New York.

[8]Department of Meteorology, University of Utah, Salt Lake City.

[9]Atmospheric Sciences Research Center, State University of New York at Albany.

Copyright 2000 by the American Geophysical Union.

Paper number 2000JD900013.
0148-0227/00/2000JD900013$09.00

Few attempts have been made to compare these two optical thicknesses largely because there are not many aircraft measurements colocated with ground-based measurements. In addition, the scattering coefficient of particles is typically measured under lower relative humidity than ambient conditions because of instrumental heating [*Ogren et al.,* 1996; *Bergin et al.,* 1997; *Remer et al.,* 1997]. Therefore a humidity correction is necessary to the scattering coefficient measured by an integrating nephelometer. The magnitude of the correction depends on the dry particle size distribution and chemical composition, as well as the state of particles [e.g., *Hänel,* 1976; *Hegg et al.,* 1993; *McInnes et al.,* 1998]. In addition, the heating process, which lowers relative humidity, can evaporate condensed-phase volatile and semivolatile chemical species such as ammonium nitrate [*Bergin et al.,* 1997]. Therefore without knowing the chemical composition, size distribution of dry particles, and state of particles the uncertainty in the corrected scattering coefficient can be significant. Measurements by *Rood et al.* [1987] show that the scattering coefficient can increase by as much as 70% by increasing relative humidity from 30% to 70%. To reduce the uncertainty in the extinction optical thickness of particles due to the relative humidity correction, *Hegg et al.* [1997] used an airborne integrating nephelometers to measure the vertical profile of the scattering coefficient at 30% and 85% relative humidity during the ascent and descent of the aircraft, respectively. They found that the extinction optical thickness of particles was systematically low by 0.04 ($\approx$ 14%) compared with the aerosol extinction optical thickness derived from an airborne Sun photometer. *Clarke et al.* [1996] computed extinction optical thicknesses of particles from vertical profiles of size distributions measured for particles between 0.15 and 7.5 $\mu$m in diameter and compared them with measured aerosol extinction optical thicknesses. The resulting optical thicknesses agree within measurement uncertainties when the particles were a mixture of ammonium sulfate, sea salt, and soot. However, when dust particles were present, the discrepancy of the optical thicknesses is greater than the uncertainty in the measurements. *Schmid et al.* [2000] compared the extinction optical thickness of particles derived from two airborne integrating nephelometers operated at different humidity conditions and a particle soot absorption photometer, with the aerosol extinction optical thickness derived from an airborne Sun photometer. They found that the extinction optical thickness of particles integrated from the extinction coefficient was smaller by 24 to 35% in the marine boundary layer. For dust particles that were present above the marine boundary layer, the difference is less than 20% when they took into account extinction by particles larger than 1.5 $\mu$m in diameter that were not sampled by the integrating nephelometers. *Remer et al.* [1997] found that the extinction optical thickness of particles derived from airborne measurements of scattering and absorption coefficients was approximately 50% less than the aerosol extinction optical thickness derived from ground-based instruments during the Sulfate Clouds and Radiation-Atlantic experiment. However, since the maximum altitude of the aircraft was 2.5 km, particles above 2.5 km might be responsible for the difference.

While earlier studies are primarily for marine aerosols, our study is based on data taken at the southern Great Plains. In this study we first derive a relation for the scattering coefficient as a function of relative humidity from data taken by two integrating nephelometers operated at the surface. Second, we compare the extinction optical thickness of particles with the aerosol extinction optical thickness derived from a multifilter rotating shadowband radiometer, a Sun photometer, and a Raman lidar for 9 days. Third, we derive the upper and lower limit of the single-scattering albedo from the result of the comparison. We then use the range of the single-scattering albedo in a sensitivity study of the top of the atmosphere albedo.

## 2. Data

### 2.1. Aircraft Data

The Gulfstream-1, which is a twin turboprop aircraft owned by the Battelle Memorial Institute, measured aerosol properties over the southern Great Plains central facility (latitude 97.48°W, longitude 36.69°N, altitude 318 m) of the Atmospheric Radiation Measurement program (operated by the Department of Energy) during intensive operation periods in April 1997, September 1997, and August 1998. The aircraft flew successive horizontal legs at different altitudes. Each leg was approximately 5 km in length. The aircraft went up to an altitude of approximately 5 km in a stacked pattern before spiraling down over the central facility. The lowest altitude at which the aircraft took measurements was approximately 100 m above the ground. The scattering coefficient was measured by an integrating nephelometer (TSI 3563 [*Anderson et al.,* 1996; *Anderson and Ogren,* 1998; *Heintzenberg and Charlson,* 1996]) at the three wavelengths of 450, 550, and 700 nm.

One error in the scattering coefficient measured by an integrating nephelometer is associated with the integration of scattered light over angle. The integrating nephelometer measures light scattered in the angle between 7° and 172° from the forward direction [*Heintzenberg and Charlson,* 1996]. Based on Mie theory, approximately 5% (10%) of the light is scattered outside of this detection range when the mode radius of an assumed lognormal number distribution is 0.3 $\mu$m (0.5 $\mu$m) and the geometric standard deviation of the distribution is 1.4. According to *Anderson et al.* [1996], when the error due to the nonlambertian property of the diffuser is taken into account, the instrument error is approximately ±5% for submicron size particles. Considering an additional uncertainty of 5% in the scattering coefficient due to volatization of dry particles [*Bergin et al.,*

1997], we estimate that the uncertainty in the measured scattering coefficient under dry conditions is less than ±10%.

The scattering coefficients measured by the integrating nephelometer were above the detection limit given by Anderson et al. (1996) except for 700 nm on April 14, 1998. During the April 1997 intensive operation period, the integrating nephelometer experienced problems associated with the in-flight measurement of the scattering coefficients of filtered air (zeroing check). As a consequence, zero checks were performed only during preflight and postflight. Therefore we treat the difference between preflight and postflight values (7.59 M $m^{-1}$ at 550 nm) as an additional uncertainty in the measured scattering coefficient for April 14.

The integrating nephelometer also measured the hemispherical backscattering coefficient at the three wavelengths. The absorption coefficient was measured by a particle soot absorption photometer (Radiance Research) at the wavelength of 565 nm. The study by *Bond et al.* [1999] indicates that a particle soot absorption photometer over-estimates absorption by 22%. Therefore we divide the absorption coefficient estimated from the particle soot absorption photometer by 1.22 for the correction. An impactor was operated upstream of both the integrating nephelometer and particle soot absorption photometer to remove particle larger than 1 $\mu$m in diameter. Therefore scattering and absorption coefficients represent for submicron particles.

### 2.2. Surface Data

While the aircraft took measurements over the central facility, ground-based instruments were operated at the site. The extinction optical thickness of the atmosphere was computed from the direct irradiance measured by a multifilter rotating shadowband radiometer at wavelengths of 415, 499, 610, 665, and 862 nm. A multifilter rotating shadowband radiometer has a rotating shadow arm, which is a strip of metal formed into a circular arc. The angular width of this shadow arm is 3.27°. When the shadow arm blocks the direct radiation, the multifilter rotating shadowband radiometer measures the downward diffuse irradiance in the discrete spectral intervals, each with a width of 10 nm. It also measures the downward total irradiance at the same wavelength intervals when the rotating shadow arm is removed from the field of view. The difference between these two values is the direct irradiance, which is used to derive the aerosol extinction optical thickness [*Harrison and Michalsky,* 1994].

In order to compute the extinction optical thickness of aerosol from multifilter rotating shadowband radiometer data, we subtract an ozone absorption optical thickness that is based on data taken at Boulder, Colorado by the Climate Monitoring and Diagnostic Laboratory of the National Oceanic and Atmospheric Administration. The monthly mean column amounts of ozone were 348 and 273 DU for April and September 1997. We use an amount of 300 DU for August 1998. These ozone amounts correspond to the absorption optical thickness of approximately 0.01 at 500 nm. However, we do not consider the absorption optical thickness of nitrogen dioxide. Estimating the column amount of nitrogen dioxide at the central facility for no more than $2.0\times10^{16}$ $cm^{-2}$ from *Luke et al.* [1992] and the cross section per molecule to be of the order of $5.0 \times 10^{-19}$ $cm^2$ [*Brasseur and Solomon,* 1984], the absorption optical thickness of nitrogen dioxide is no more than 0.01. We also neglect stratospheric aerosols because the optical thickness of stratospheric aerosols is probably less than 0.01 at 500 nm based on Stratospheric Aerosol and Gas Experiment II data [*Thomason et al.,* 1997a, b]. Based on this and the error in the calibration, we estimated that the uncertainty in the aerosol extinction optical thickness derived from the multifilter rotating shadowband radiometer is ±0.01.

In addition to the multifilter rotating shadowband radiometer, a Sun photometer (Cimel Sun photometer) was operated at the site as a part of the Aerosol Robotic Network. The Sun photometer measures the extinction of the direct irradiance in the 1.2 degree full angle field of view at wavelengths of 340, 380, 440, 500, 670, 870, and 1020 nm each with a width of 10 nm [*Holben et al.,* 1998]. We also estimate the uncertainty in the extinction optical thickness derived from the Sun photometer is ±0.01.

The scattering coefficient was also measured at the central facility by an integrating nephelometer (TSI 3563) at ≈ 20% relative humidity [*Bergin et al.,* 2000]. In addition to this integrating nephelometer, a second integrating nephelometer was installed in December 1998 to measure the scattering coefficient as a function of relative humidity. This is done by controlling relative humidity at upstream of the integrating nephelometer ranging from 40% to 90% using a procedure described by *Rood et al.* [1987].

The absorption coefficient at 565 nm is measured by a particle soot absorption photometer at the central facility. Further, a Raman lidar [*Goldsmith et al.,* 1998] was operated during intensive operation periods in September 1997 and August 1998. The Raman lidar measures the extinction coefficients profile at 355 nm, which can be integrated with respect to height in order to estimate the extinction optical thickness of aerosol at 355 nm. Among these data taken during intensive operation periods in April 1997, September 1997, and August 1998, we select data taken on April 14, 1997, September 27 and September 29, 1997, and August 14, 15, 17, 18, 19 and 20, 1998.

### 2.3. Meteorological Conditions

A cold front passed over the central facility on April 11, 1997, early in the morning, which produced approximately 60 mm of precipitation at the site. A high-

pressure system over Arizona moved to the east, and the center passed over Oklahoma on April 13 before it moved to the east of Oklahoma on April 14. April 14 was a cloudless day. The atmospheric profile at 1800 UT (local time is 5 hour behind universal time) on April 14 shows that the potential temperature and dew point were nearly constant from the surface to $\approx 1.2$ and $\approx 1.5$ km, respectively. These data indicate that the height of the boundary layer was 1.2 to 1.5 km. Surface isobars were oriented southwest to northeast at 1200 UT on April 14, and we regard the air mass as maritime [i.e., *Ryan et al.*, 1992]. The surface wind was southerly on April 14, with a maximum 30 min averaged wind speed of about 9 $\mathrm{m\,s^{-1}}$ in the afternoon.

On September 26, 1997, 1200 UT, a high-pressure system was located over Texas. The high moved to the east of Oklahoma on September 27, which was a clear day with southerly winds at the surface. The maximum 30 min averaged wind speed of about 10 $\mathrm{m\,s^{-1}}$ occurred in the afternoon. The atmospheric profile at 1700 UT on September 27 shows that the potential temperature was nearly constant from the surface to $\approx 0.5$ km altitude. Surface isobars were oriented southwest to northeast at 1200 UT on September 27 and we also regard this air mass as maritime. A weak front passed over the site on September 28 but no precipitation was reported at the site. After the front passed, a high-pressure system moved from the northwest over Oklahoma on September 29. September 29 was clear with southwesterly winds at the surface. The maximum 30 min averaged wind speed was about 8 $\mathrm{m\,s^{-1}}$, which occurred in the afternoon. The atmospheric profile at 1900 UT on September 29 shows that the potential temperature is a minimum at $\approx 0.75$ km.

Between August 14 and 20, skies were cloudless in the early morning with fair weather cumulus clouds forming in the late morning or early afternoon. The wind was predominantly southerly with a maximum 30 min averaged wind speed of about 9 $\mathrm{m\,s^{-1}}$ for the period. For most of nine cases selected from these intensive operation periods, the relative humidity increases with height in the boundary layer as indicated by three independent measurements (Figure 1). The relative humidity of the atmosphere for all nine cases is less than 70% except at the upper part of the boundary layer.

## 3. Method and Results

### 3.1. Scattering Coefficient as a Function of Relative Humidity

As previously discussed, scattering coefficients were measured at lower relative humidity than ambient conditions (Figure 1). When a particle is hygroscopic, its equilibrium size increases with relative humidity in a range above its deliquescent point before being activated to become a droplet. In addition, since a particle can be supersaturated with respect to salts below the deliquescent point (metastable state), the size of the particle can be larger than the dry particle. Therefore the scattering coefficient of particles measured at low relative humidity can be either significantly different or the same compared with the actual scattering coefficient of the particles in the atmosphere even below the deliquescent point.

The extinction optical thickness of particles integrated from the scattering and absorption coefficient $\tau_{\mathrm{p}}$ is given by

$$\tau_{\mathrm{p}}(\lambda, RH) = \int_0^{5\,km} [\sigma_{\mathrm{sp}}(\lambda, z) F_{\mathrm{sca}}(\lambda, RH) + \sigma_{\mathrm{ap}}(\lambda, z) F_{\mathrm{abs}}(\lambda, RH)]\, dz, \tag{1}$$

where $\sigma_{\mathrm{sp}}$ and $\sigma_{\mathrm{ap}}$ are the scattering and absorption coefficients, respectively, measured under dry conditions, $F_{\mathrm{sca}}$ and $F_{\mathrm{abs}}$ are the humidity corrections to these coefficients, and $RH$ is the relative humidity of the atmosphere [i.e., *Hegg et al.*, 1997; *Bergin et al.*, 2000]. While we assume that $F_{\mathrm{abs}}$ is unity, we need to estimate $F_{\mathrm{sca}}$ in order to compute $\tau_{\mathrm{p}}$. As previously mentioned, $F_{\mathrm{sca}}$ depends on several factors including the size distribution and chemical composition of dry particles, as well as state of particles, which were not measured in our study. Therefore we estimate $F_{\mathrm{sca}}$ using two integrating nephelometers operated under different relative humidity conditions by

$$F_{\mathrm{sca}}(\lambda, RH) = \frac{\sigma_{\mathrm{sp}}(\lambda, RH)}{\sigma_{\mathrm{sp,ref}}(\lambda)}, \tag{2}$$

where $\sigma_{\mathrm{sp}}(\lambda, RH)$ and $\sigma_{\mathrm{sp,ref}}(\lambda)$ is the scattering coefficient measured at wet and dry conditions, respectively. We use data taken at the surface from December 1998 to January 1999 to derive $F_{\mathrm{sca}}(\lambda, RH)$. In order to correct the scattering coefficient measured by the aircraft, we sort $F_{\mathrm{sca}}(\lambda, RH)$ using bins with a 5% relative humidity increment for all three wavelengths (Figure 2). We then interpolate these values at the ambient relative humidity for the correction. The resulting $F_{\mathrm{sca}}(550, 80)$ is $1.72 \pm 0.13$, which is in agreement with similar measurement of anthropogenic particles by *McInnes et al.* [1998] at Sable Island and by *Rood et al.* [1987] at Riverside, California in August and September for particles less than 2 $\mu$m in diameter.

We compute $\tau_{\mathrm{p}}$ by applying these relations for $F_{\mathrm{sca}}$ in (1) when the ambient relative humidity is greater than 50%. Since $F_{\mathrm{sca}}$ is based on data taken at the surface in winter, we assume that chemical components and size distribution of dry particles in the atmospheric column are similar to those at the surface for all seasons by applying this relation as a correction to the scattering coefficient measured aloft.

### 3.2. April and September 1997 Case Study

We average the scattering coefficient measured by the integrating nephelometer equipped on the aircraft over

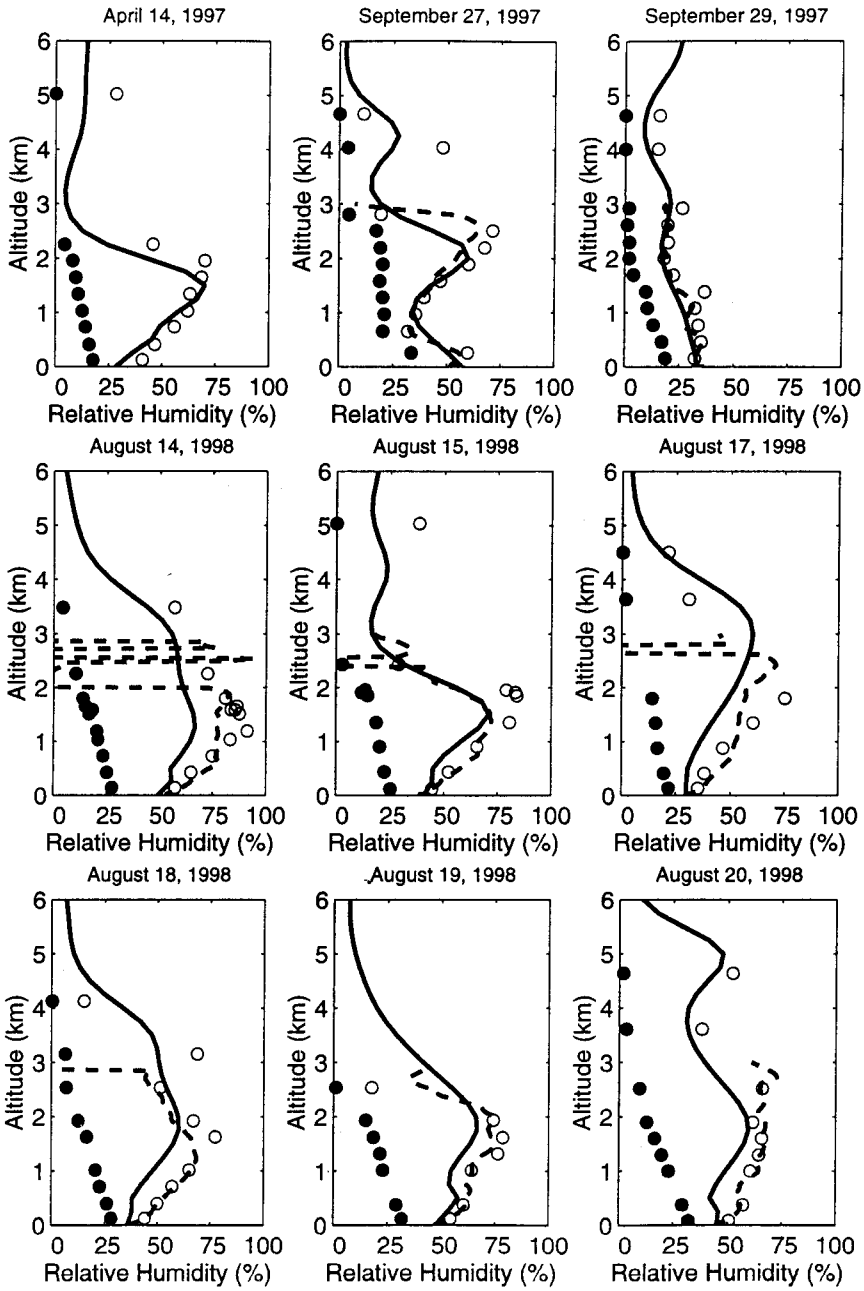


**Figure 1.** Relative humidity profile interpolated from soundings (solid line) for the nine case study days. Open and solid circles indicate the ambient relative humidity measured at the aircraft and the relative humidity inside the integrating nephelometer, respectively. The dashed line in the September 1997 and August 1998 plots indicates the relative humidity profile derived from the Raman lidar.

each flight leg. The averaged scattering coefficient at 550 nm for 3 days shows that although the maximum scattering coefficient occurs in the boundary layer, scattering by particles in the free troposphere is not negligible (Figure 3). The fraction of the scattering optical thickness by particles in the boundary layer to that in the entire column is approximately 0.4, 0.4, and 0.3 for April 14, September 27, and September 29, respectively. This result is consistent with the result of *Bergin et al.* [2000] who also show significant scattering by particles above the boundary layer at the same site. The small standard deviation for each leg indicates that the horizontal variation of the optical properties of the particles is small compared with the variation in the vertical. Another feature is that the scattering coefficient measured at the surface is 18%, 32%, and 55% smaller relative to the value measured by the aircraft at the lowest altitude for April 14, September 27, and September 29, respectively.

The scattering optical thickness of particles estimated from the scattering coefficient averaged over each leg and from the values obtained by spiraling down over

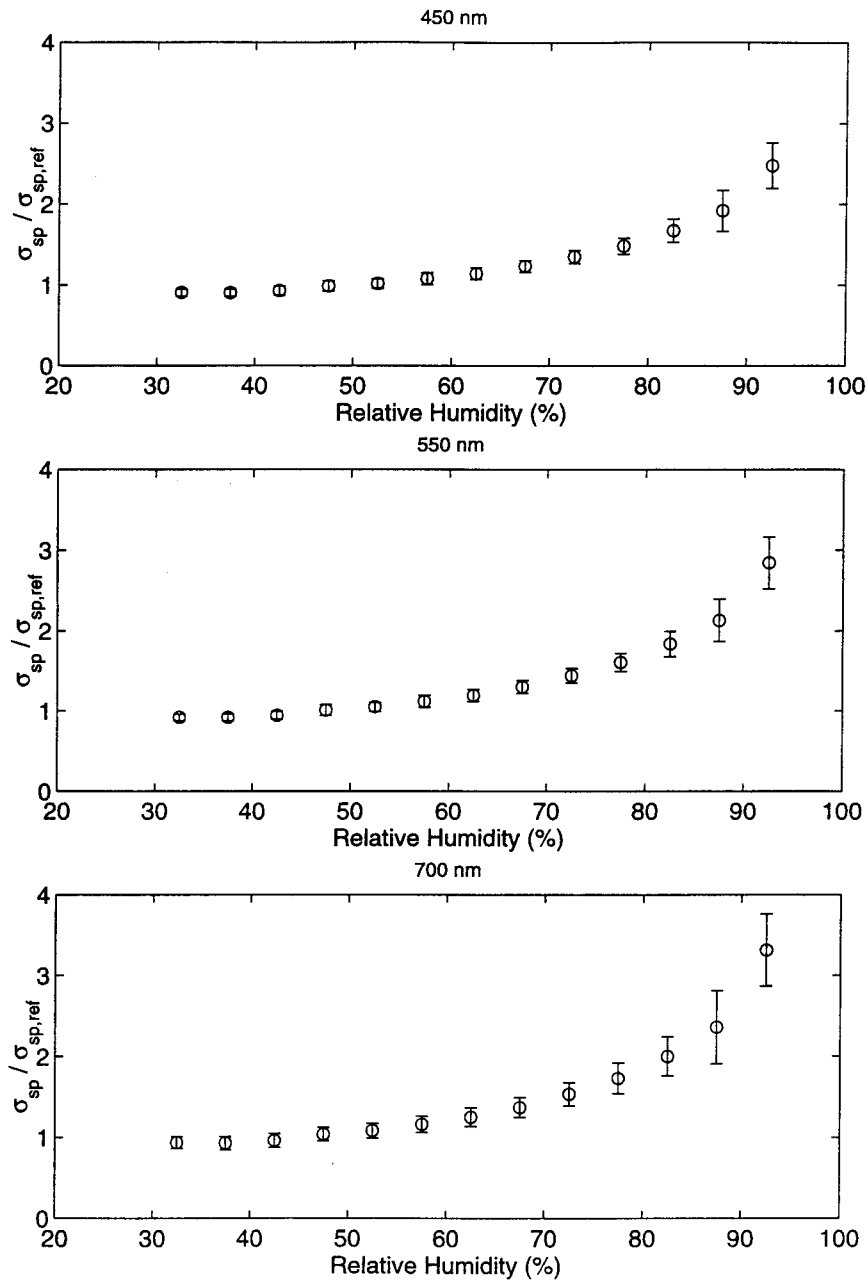


**Figure 2.** Ratio of the scattering coefficient measured under wet conditions to that measured under dry conditions as a function of the relative humidity of wet conditions for the three wavelengths. Open circles and error bars indicate averaged values and standard deviations for every 5% relative humidity intervals.

the central facility differ by less than 10% for all 3 days. This indicates that the optical properties of dry particles were nearly constant with time during the flight time of approximately 2 hours.

The humidity correction by (1) and (2) increases $\tau_p$ by $7 \times 10^{-3}$ and $2 \times 10^{-3}$ at 550 nm corresponding to 6% and 4% of $\tau_p$ on April 14 and September 27, respectively. Since the relative humidity of the atmosphere is less than 50% on September 29 (Figure 1), $\tau_p$ is not altered by applying the humidity correction to the data. Both the single-scattering albedo $\varpi$ estimated from the scattering and absorption coefficient and the ratio of the hemispheric backscattering coefficient to the total scattering coefficient $b$ are nearly constant with height on April 14 and September 27 (Figure 4 and 5). Note that we used the absorption coefficient measured at 565 nm for the computation of $\varpi$ at 550 nm and the values used for Figure 4 are not including the humidity correction. The ratios of the scattering optical thickness to $\tau_p$ at 550 nm are 0.92, 0.85, and 0.83 for April 14, September 27, and September 29, respectively. These values can be interpreted as an averaged single-scattering albedo

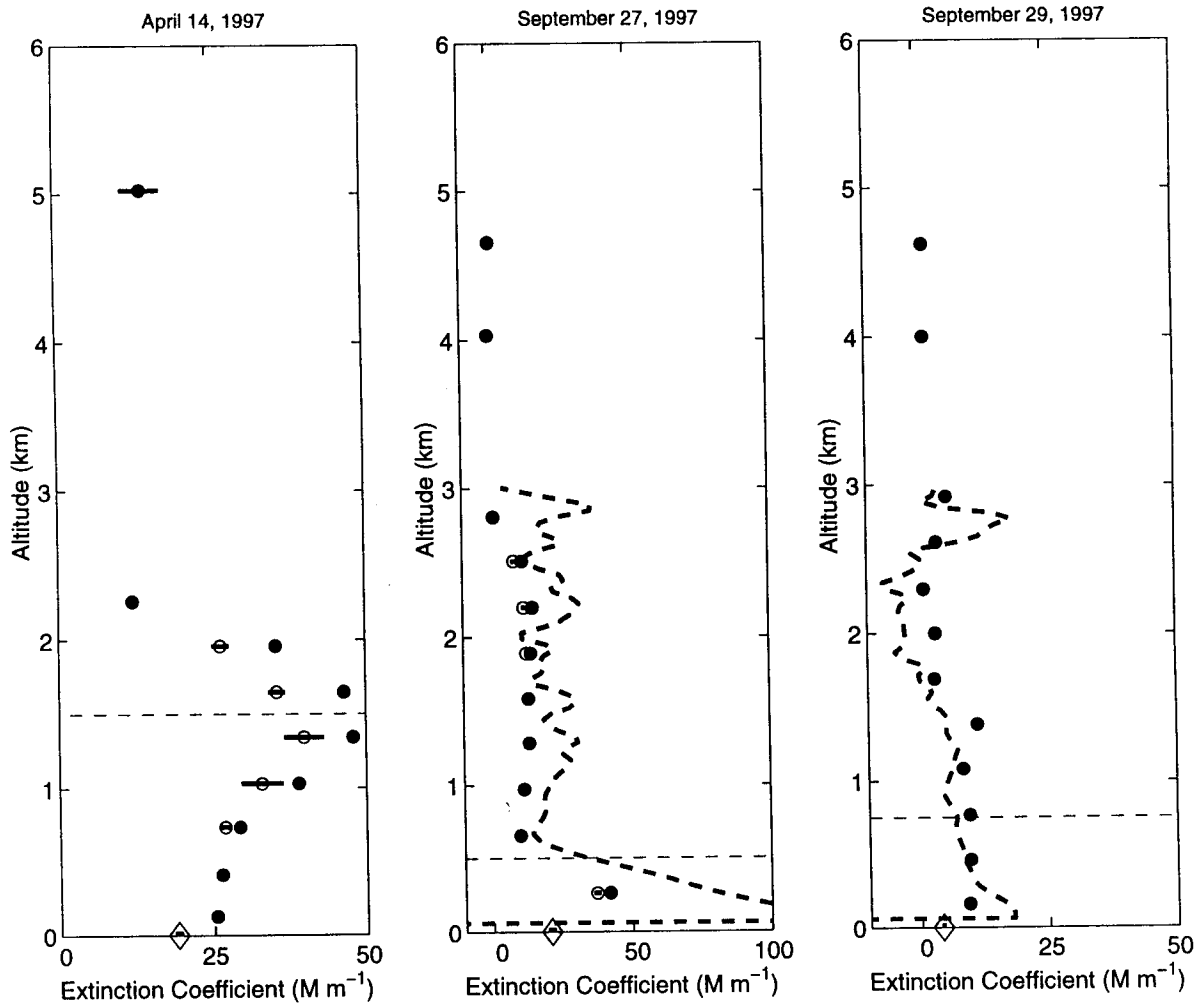


**Figure 3.** Extinction coefficients at 550 nm, which are the sum of the scattering coefficient measured by the integrating nephelometer and the absorption coefficient measured by the particle soot absorption photometer. Solid and open circles are with and without humidity corrections to the nephelometer data, respectively. Horizontal lines through the open circles indicate the standard deviation for each averaged value. The thin dashed line indicates the estimated height of the boundary layer. The thick dashed lines in September 1997 plots are the extinction coefficient profile at 550 nm estimated from the Raman lidar averaged over each flight period.

of dry particles estimated from aircraft measurements. According to *Sheridan and Ogren* [1999], the single-scattering albedo estimated from similar aircraft measurements over the Great Plains varies from 0.91 to 0.96. The single-scattering albedos for September 27 and 29 cases are lower than those estimated by *Sheridan and Ogren* [1999]. Since both the single-scattering albedo and $\tau_p$ for the September 29 case are the lowest among the three cases and the variation of the single-scattering albedo with height for the September 29 case is the largest, one possible reason for the difference is that the limitation of the instruments to estimate the single-scattering albedo at low scattering and absorption coefficients. When the scattering and absorption coefficients are small, the error in the single-scattering albedo increases even if the error in these coefficients stay the same.

The single-scattering albedo $\varpi$ measured at the surface are greater by 0.04, 0.03, and 0.04 for April 14, September 27, and September 29, respectively, compared with those measured by the aircraft at the lowest altitude (Figure 4). Note that $b$ is also measured under dry conditions. Therefore the constant value of $b$ suggests that the sizes of the dry particles are nearly constant with height. The values of $b$ measured at the surface are greater by 0.05, 0.04, and 0.06 for April 14, September 27, and September 29, respectively, compared with those measured by the aircraft at the lowest altitude (Figure 5).

The Raman lidar operated at the central facility measured the extinction coefficient at 355 nm. In order to compare the extinction coefficient derived from the Raman lidar with the extinction coefficient of particles at 550 nm derived from the aircraft measurements, we

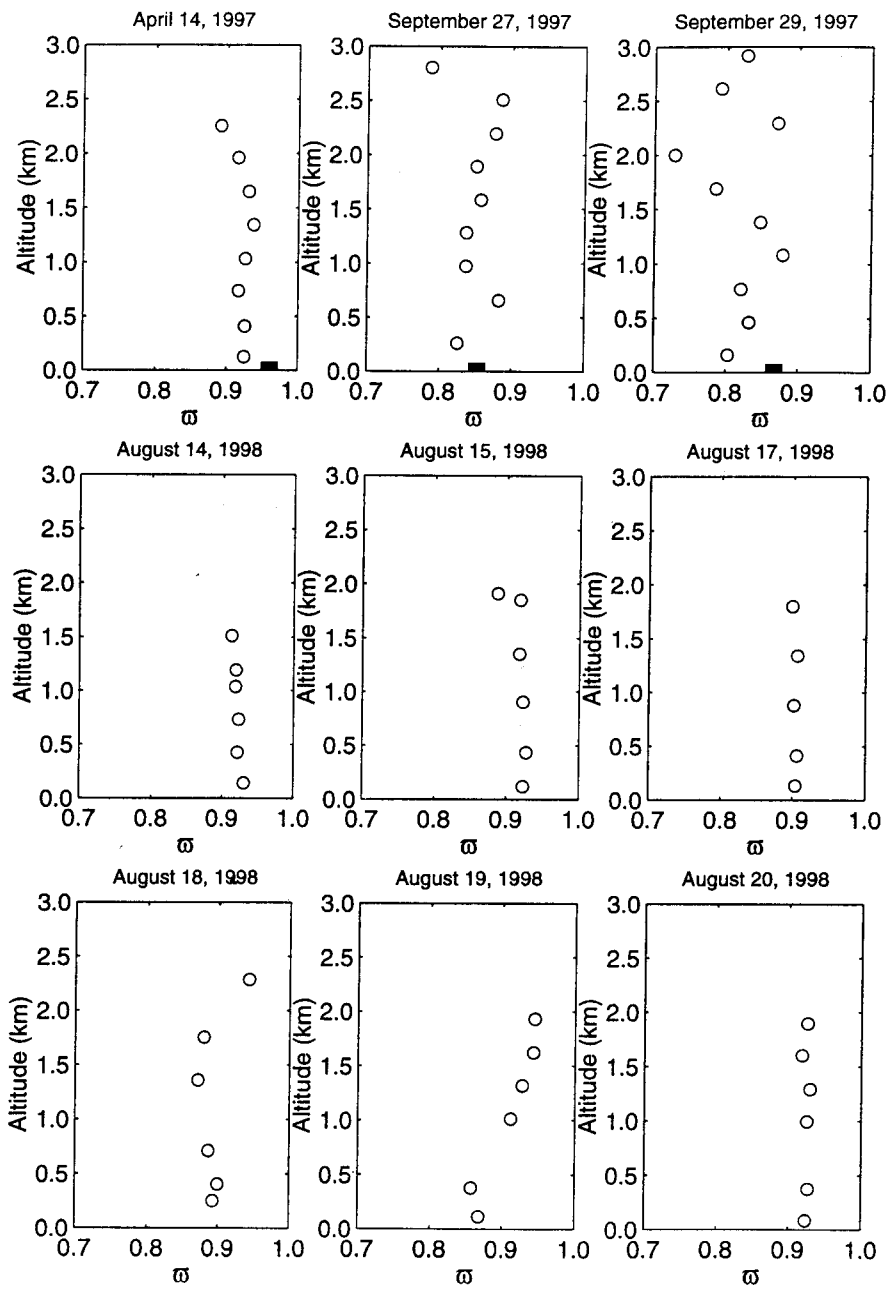


**Figure 4.** Single-scattering albedo $\varpi$ profile obtained from the scattering coefficient measured by the integrating nephelometer and the absorption coefficient measured by the particle soot absorption photometer using aircraft data (open circles) and surface data (solid squares), respectively. There are no surface data available for August 1998.

scale the extinction coefficient derived from the Raman lidar $\sigma_{\mathrm{sp,rl}}$ by

$$\sigma_{\mathrm{sp,rl}}(550) = \frac{\tau(500)}{\tau(340)}\sigma_{\mathrm{sp,rl}}(355), \tag{3}$$

where $\tau(340)$ and $\tau(500)$ is the aerosol optical thickness derived from the Sun photometer at wavelengths of 340 and 500 nm, respectively. When the Sun photometer was not operated during the flight period (August 18), we use the relation

$$\sigma_{\mathrm{sp,rl}}(550) = \left(\frac{550}{355}\right)^{-l}\sigma_{\mathrm{sp,rl}}(355), \tag{4}$$

where $l$ is the exponent fitted to the aerosol optical thickness $\tau$ derived from the multifilter shadowband radiometer by the Lundholm relation

$$\tau = \alpha\lambda^{-l}, \tag{5}$$

where $\lambda$ is the wavelength. The Lundholm relation is often referred to as the Ångström relation, although

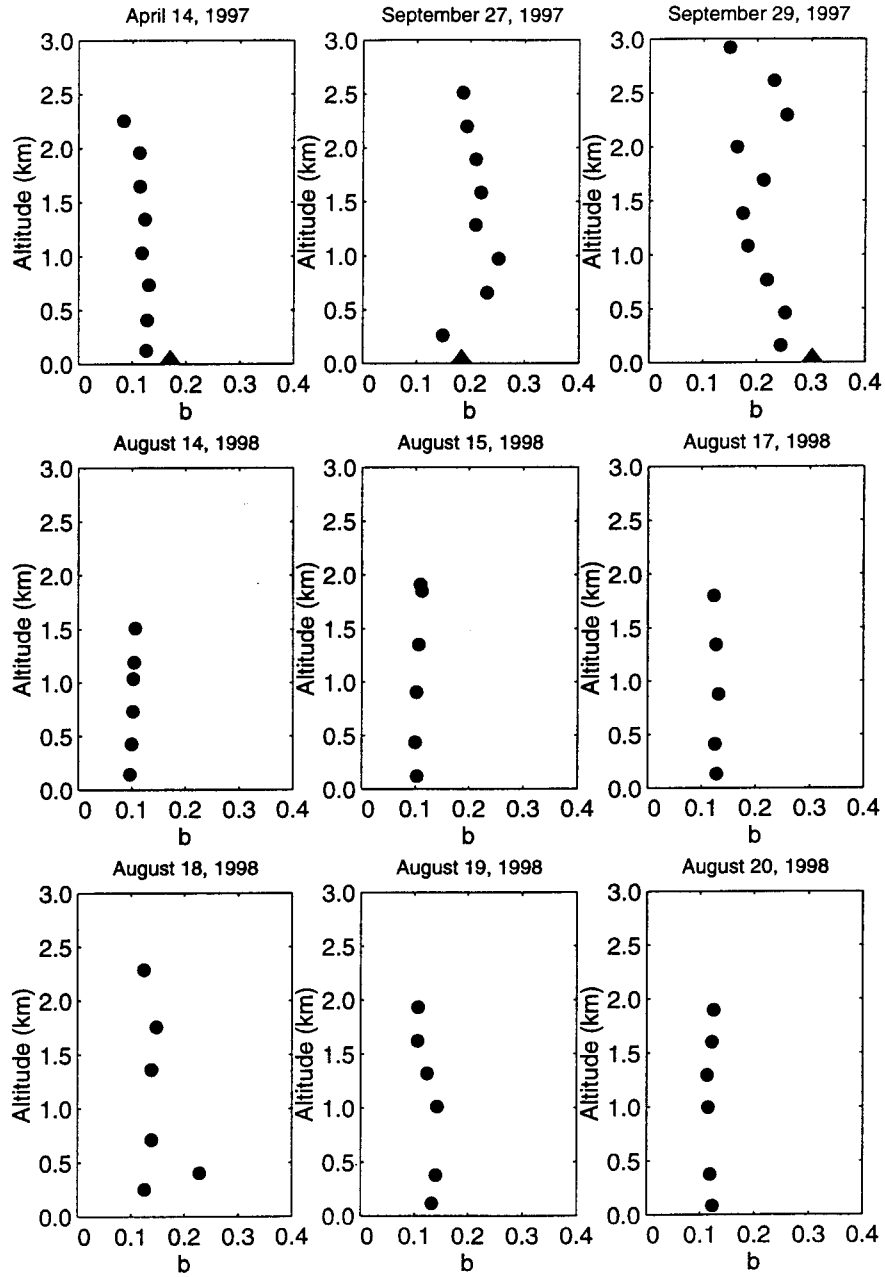


**Figure 5.** Ratio of the backward hemisphere scattering to the total scattering $b$ at 550 nm estimated from aircraft data (solid circles) and surface data (solid triangles), respectively. There are no surface data available for August 1998.

*Ångström* [1929] acknowledges that the idea was not his original.

In order to estimate the extinction optical thickness $\tau_p$ at 450 and 700 nm, we assume that the absorption coefficient is constant with wavelength; we use the absorption coefficient measured at 565 nm for the value at 450 and 700 nm. Comparisons of $\tau_p$ with the aerosol extinction optical thickness derived from the multifilter rotating shadowband radiometer ($\tau_{mfrsr}$ hereinafter) show that $\tau_p$ is smaller for the 3 days (Figure 6). The differences at 550 nm are 0.01, 0.02, and 0.01 for April 14, September 27, and September 29, respectively, which correspond to 10%, 32%, and 28% of $\tau_{mfrsr}$.

### 3.3. August 1998 Case Study

The averaging procedure for the scattering and absorption coefficients is the same as for the previous three cases (section 3.2); the scattering coefficient is averaged over each flight leg. Figure 7 shows the profile of the extinction coefficient of particles with and without the humidity correction by (1) and (2). The extinction coefficient corrected for ambient relative humidity is signif-

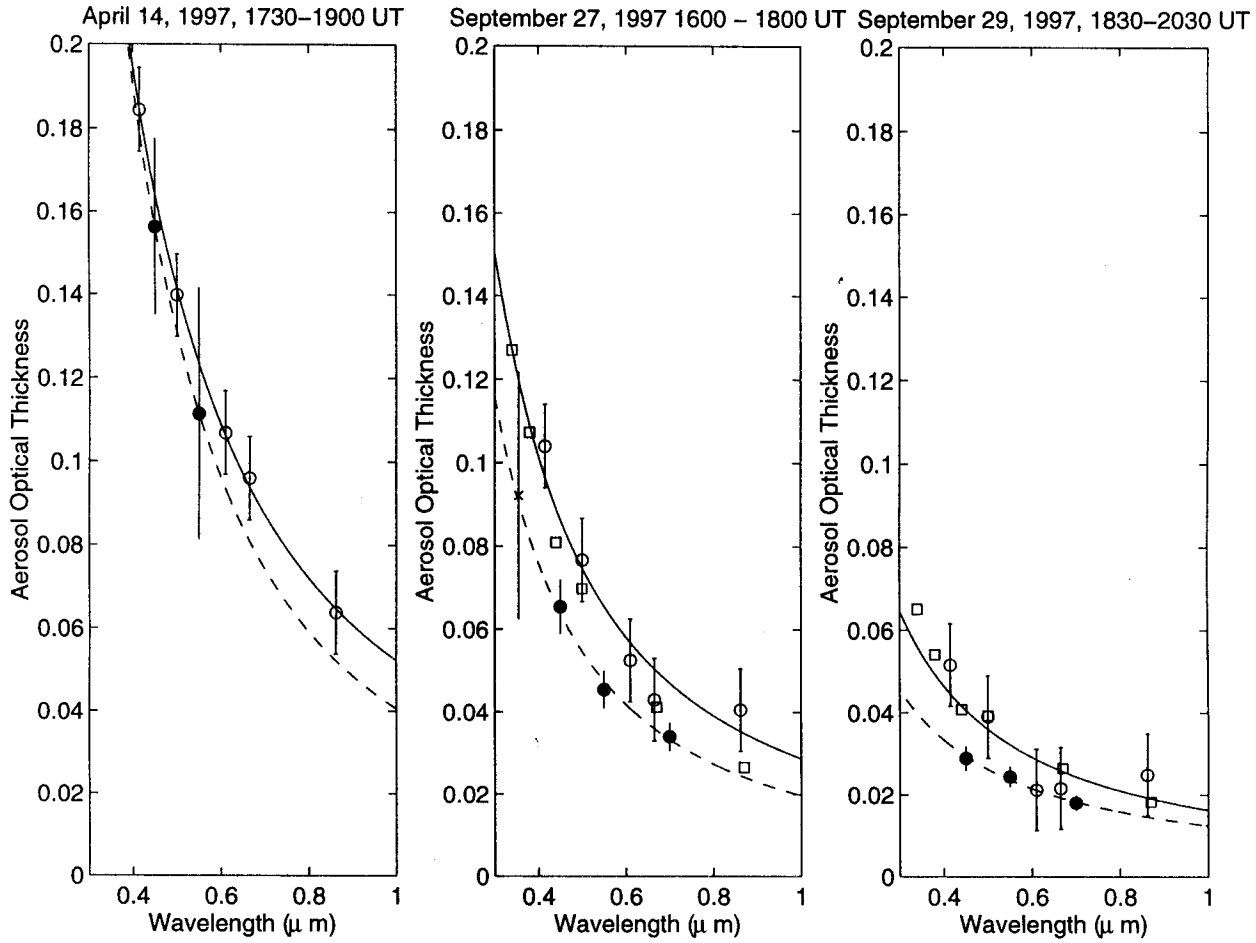


**Figure 6.** Aerosol extinction optical thickness obtained from the multifilter rotating shadowband radiometer (MFRSR) (open circles) and the Sun photometer (squares) as a function of wavelength averaged over flight periods. Solid circles indicate the extinction optical thickness obtained by summing the particle scattering and absorption coefficients measured by the airborne integrating nephelometer and particle soot absorption photometer, respectively. The error bar indicates the estimated uncertainty in the nephelometer-derived extinction optical thickness and ±0.01 uncertainty for the MFRSR-derived extinction optical thickness. The solid and dashed line are the result of fitting a Lundholm relation to the MFRSR and aircraft data, respectively. The extinction optical thickness derived from the Raman lidar at 355 nm on September 27, 1997, is also plotted (cross) with a vertical bar indicating the variation during the flight period.

icantly greater than the extinction coefficient measured at low relative humidity, especially at the top of the boundary layer where ambient relative humidity tends to be the highest.

The extinction coefficient derived from the Raman lidar shown in Figure 7 is the value averaged over each flight period after the values are scaled using (3) or (4). Both aircraft- and Raman lidar-derived profiles have maxima approximately the same height above ground level. However, the profiles derived from the airborne integrating nephelometer have not resolved a sharp increase in the extinction coefficient near 2 km above ground level on August 14 and 15. The leg-averaged extinction coefficients do not capture the increase at 2.5 km on August 17 because the aircraft did not fly at that level. The leg-averaged extinction coefficient on August 19 has a maximum at 2 km above ground level. However, the value is smaller than that derived from the Raman lidar.

The aerosol extinction optical thickness derived from the multifilter rotating shadowband radiometer $\tau_{\mathrm{mfrsr}}$ during flight periods on 4 of the 6 days does not appear to be affected by clouds based on the cloud screening process given by *Harrison and Michalsky* [1994]. Assuming the absorption coefficient is constant with wavelength, we are able to obtain the extinction optical thickness of particles at three wavelengths. For all 4 days, the extinction optical thicknesses of particles $\tau_{\mathrm{p}}$ is smaller than $\tau_{\mathrm{mfrsr}}$ (Figure 8). The difference varies from 0.03 to 0.07, which corresponds to 25% to 31% of $\tau_{\mathrm{mfrsr}}$. The value of $\tau_{\mathrm{p}}$ at 550 nm is 72% of $\tau_{\mathrm{mfrsr}}$ when those are averaged over the 4 days (Table 1).

Since fair weather cumulus clouds formed during the later part of all these flights, the particle sizes at the

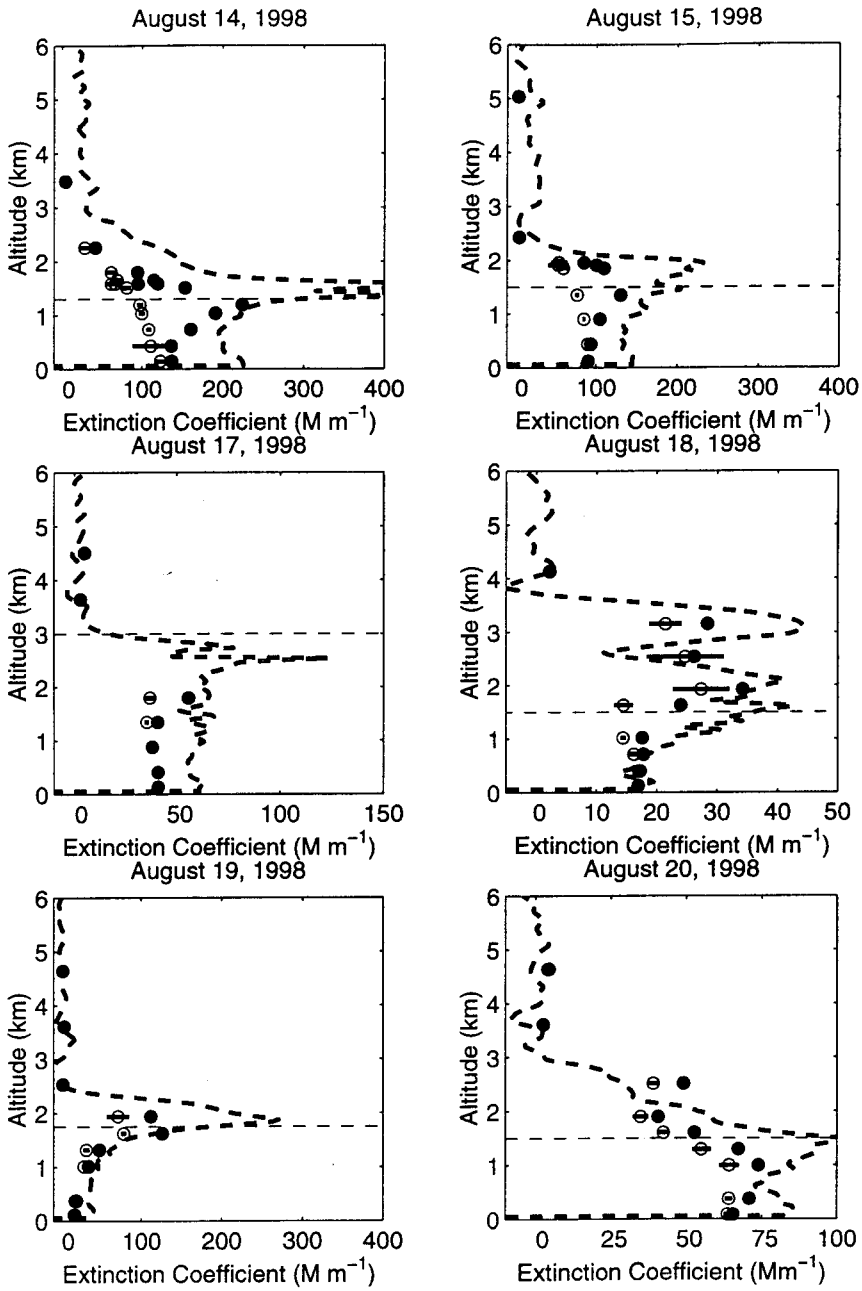


**Figure 7.** Same as Figure 3, but for August 1998.

top of the boundary layer changed rapidly during these flights. Larger standard deviations, indicated by thick horizontal bars at the top of the boundary layer in Figure 7, suggest a larger horizontal variability in the scattering property of the particles. These spatial and, perhaps, temporal variations can contribute to the difference between the airborne- and Raman lidar-derived extinction coefficient profiles. In addition, the integrating nephelometer samples submicron particles and misses particles the diameter of which is greater than 1 $\mu$m; this can also be responsible for the difference. Furthermore, if the particles in the atmosphere contain more hygroscopic material than the particles present at the surface, we will underestimate $F_{\mathrm{sca}}$.

## 4. Discussion

### 4.1. Comparison of Extinction Optical Thicknesses

The agreement between $\tau_{\mathrm{mfrsr}}$ and $\tau_{\mathrm{p}}$ depends largely on the correction of the scattering coefficient measured under lower relative humidity conditions. If particles are completely hygroscopic, the size can change by up to approximately 20% when they are dried from 60% relative humidity to 20% relative humidity depending on the state (dry or metastable) of particles [e.g., *Tang and Munkelwitz,* 1994]. When a particle is small compared with the wavelength, the scattering cross section is proportional to the sixth power of the radius; when

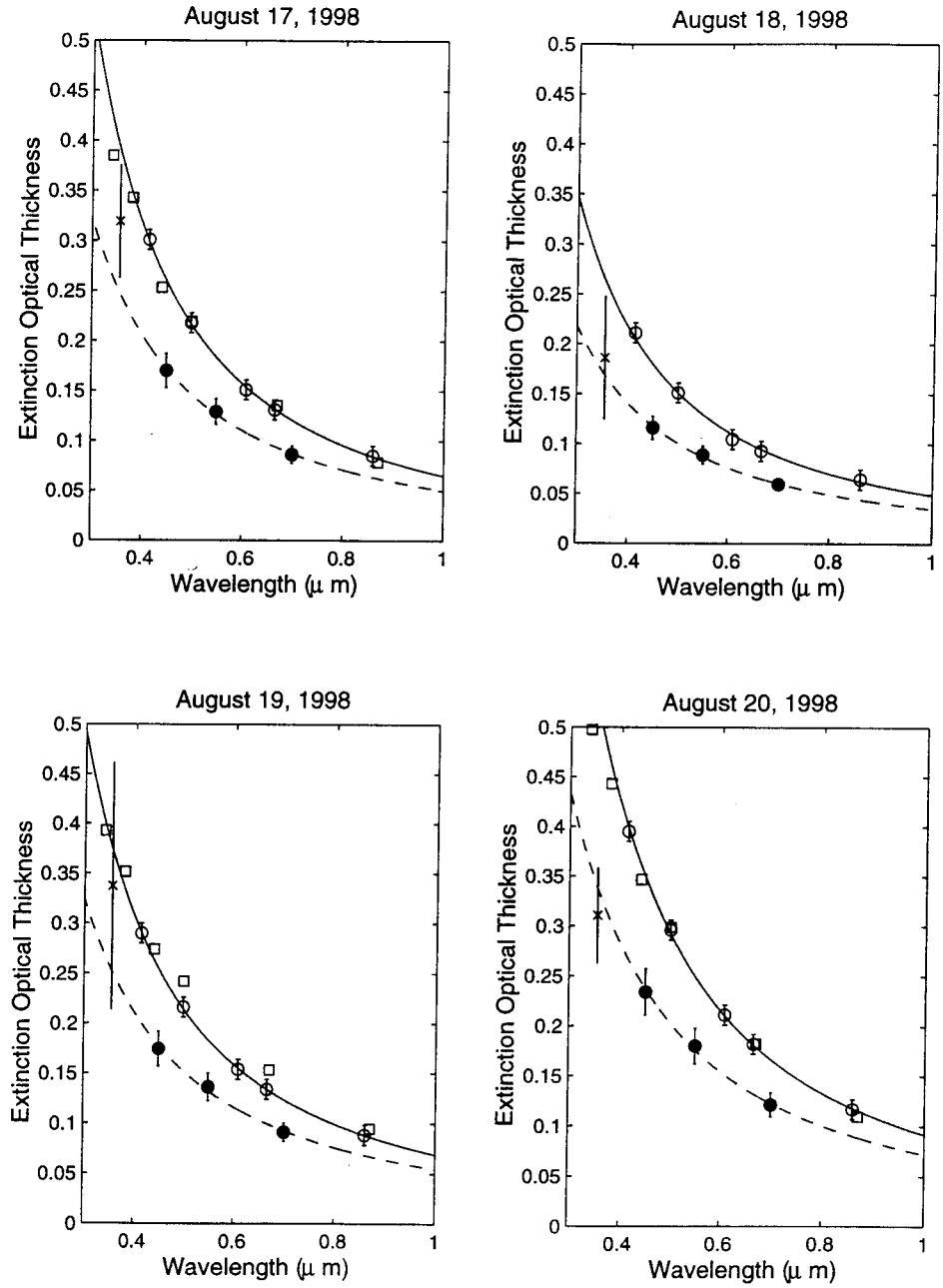


**Figure 8.** Same as Figure 6, but for August 1998.

a particle is large compared with the wavelength, the scattering cross section is proportional to the square of the radius [*Bohren and Huffman,* 1983]. Therefore a 20% increase in size corresponds to a factor of 1.4 to 3 increase in the scattering coefficient depending on the size distribution of the dry particles. In order to reduce the uncertainty in the humidity correction, we empirically estimate $F_{sca}$. The relation of $F_{sca}$ estimated from two integrating nephelometers operated under two different relative humidity conditions at the surface indicates that the water uptake by particles is less than that for purely hygroscopic particles. This suggests that some fraction of particles are either dry or not hygroscopic.

Given instrumental errors and uncertainties in the retrieved extinction optical thicknesses, the difference between $\tau_p$ and $\tau_{mfrsr}$ on April 14, September 27, and September 29 is not significant (Figure 6). However, the larger differences obtained during August 1998 cannot be explained by these uncertainties.

There are several possible reasons for the discrepancy between $\tau_p$ and $\tau_{mfrsr}$ for the August cases including (1) the fact that the sampling efficiency of the aircraft sampling inlet is not known and exclude particles greater than 1$\mu$m upstream of the integrating nephelometer and particle soot absorption photometer, (2) cloud contamination in the multifilter shadowband radiometer data, (3) large temporal and spatial variations of the particle

**Table 1.** Comparison of the Extinction Optical Thickness at 550 nm

| Date | Time, UT | MFRSR | Cimel | Aircraft | Raman Lidar | Boundary Layer Average Relative Humidity, % |
|---|---|---|---|---|---|---|
| April 14, 1997 | 1730 - 1900 | 0.125 | - | 0.113 | - | 51.5 |
| Sept. 27, 1997 | 1600 - 1800 | 0.066 | 0.058 | 0.045 | 0.047 (0.092) | 45.9 |
| Sept. 29, 1997 | 1830 - 2030 | 0.032 | 0.034 | 0.023 | - | 34.1 |
| Aug. 14, 1998 | 1830 - 2030 | - | 0.379 | 0.321 | 0.497 (0.737) | 72.8 |
| Aug. 15, 1998 | 1900 - 2100 | - | 0.315 | 0.230 | 0.396 (0.593) | 61.3 |
| Aug. 17, 1998 | 1800 - 1940 | 0.183 | 0.185 | 0.127 | 0.182 (0.319) | 51.5 |
| Aug. 18, 1998 | 1700 - 1845 | 0.116 | - | 0.087 | 0.092 (0.186) | 61.0 |
| Aug. 19, 1998 | 1600 - 1800 | 0.183 | 0.204 | 0.135 | 0.208 (0.338) | 66.1 |
| Aug. 20, 1998 | 1600 - 1800 | 0.249 | 0.250 | 0.178 | 0.187 (0.311) | 59.8 |

Numbers in parentheses indicate the aerosol optical thickness at 355 nm.

extinction coefficients, and (4) errors in the humidity correction to the integrating nephelometer data given by (2).

When we fit the wavelength-dependent optical thickness by (5), we can infer the size of particles by the Lundholm exponent $l$. In order to find whether the nephelometer missed large particles, we compute $l$ from the wavelength-dependent extinction optical thickness derived from the multifilter rotating shadowband radiometer and Sun photometer (Table 2) and compare with $l$ derived from $\tau_p$. If the integrating nephelometer missed larger particles, $l$ derived from $\tau_p$ should be larger than that derived from the multifilter rotating shadowband radiometer and Sun photometer. The result, however, does not support the hypothesis (Table 2). In order to investigate the error in the Lundholm exponent $\sigma_l$ due to the error in the extinction optical thickness, we use [*Wilks,* 1995]

$$\sigma_l = \left[ \frac{\sum_{i=1}^{n} e_i^2}{(n-2)\sum_{i=1}^{n}(\ln \lambda_i - \overline{\ln \lambda})^2} \right]^{1/2}, \qquad (6)$$

where $e_i$ is the error of the Lundholm relation, $n$ is the number of wavelengths $\lambda_i$ used to fit the Lundholm relation, and $\overline{\ln \lambda}$ is the average of the logarithm of the wavelengths. When we use $\epsilon_i/\tau_i$ for $e_i$ and the uncertainty in the optical thickness of 0.01 for $\epsilon_i$, $\sigma_l$ is approximately 0.2. Therefore the difference between $l$ derived from the multifilter rotating shadowband radiometer and integrating nephelometer shown in Table 2 is not significant. Therefore we cannot conclude whether the integrating nephelometer misses large particles from the Lundholm exponent.

**Table 2.** Comparison of the Lundholm Exponents

| Date | Time, UT | MFRSR | Aircraft | Cimel |
|---|---|---|---|---|
| April 14, 1997 | 1730 - 1900 | 1.44 | - | - |
| Sept. 27, 1997 | 1600 - 1800 | 1.38 | 1.47 | 1.67 |
| Sept. 29, 1997 | 1830 - 2030 | 1.15 | 1.08 | 1.31 |
| Aug. 14, 1998 | 1830 - 2030 | - | 1.29 | 1.49 |
| Aug. 15, 1998 | 1900 - 2100 | 1.51 | 1.33 | 1.48 |
| Aug. 17, 1998 | 1800 - 1940 | 1.73 | 1.54 | 1.69 |
| Aug. 18, 1998 | 1700 - 1845 | 1.63 | 1.52 | - |
| Aug. 19, 1998 | 1600 - 1800 | 1.63 | 1.48 | 1.51 |
| Aug. 20, 1998 | 1600 - 1800 | 1.67 | 1.49 | 1.61 |

With regard to cloud contamination, the Raman lidar did not detect clouds for these periods. The vertical lines attached to the extinction optical thicknesses derived from the Raman lidar in Figure 8 indicate the variations in the extinction optical thickness during the 2 hour flight periods. The large variability suggests that the size of particles changed rapidly if we assume that the number concentration did not change very much.

While we are not able to address the reason of the difference between these extinction optical thicknesses further, we can check whether $\tau_{mfrsr}$ gives observed direct irradiances by pyrheliometers when it is used for computations of the direct irradiance. The direct irradiance does not depend on the chemical composition of particles and is almost independent of their size. However, the direct irradiance does depend on the water vapor amount in the atmosphere. We use a water vapor profile interpolated from soundings at the site combined with the $k$-distribution method and correlated-$k$ approximation in order to compute the absorption optical thickness of water vapor [*Kato et al.,* 1999]. We use (5) to fit $\tau_{mfrsr}$ to compute the extinction optical thickness of aerosol at 32 wavelengths over the solar spectrum from 0.24 to 4.6 $\mu$m [*Kato et al.,* 1997; *Kato et al.,* 1999]. We use a formula given by *Hansen and Travis* [1974] to compute the scattering optical thickness of molecules. The resulting direct irradiance is 1.3% larger than the average of the direct irradiance measured by two pyrheliometers located at the central facility when their measurements between 1500 and 1700 UT are averaged over 4 days. Since the Atmospheric Science Division of the NASA Langley Research Center deployed a cavity radiometer at the central facility on August

**Table 3.** Estimated Single-Scattering Albedo and Sensitivity of the Albedo of the Atmosphere

| Date | Estimation Source | Height Range, km | Fraction of Optical Thickness | $\varpi$ | Albedo of the Atmosphere $\mu_0$=0.867 | Albedo of the Atmosphere $\mu_0$=0.5 |
|---|---|---|---|---|---|---|
| April 14 | Aircraft | 0.0 - 1.0 | 0.3 | 0.927 | | |
| | Aircraft | 1.0 - 1.6 | 0.4 | 0.945 | | |
| | Aircraft | 1.6 - 2.0 | 0.3 | 0.942 | 0.193 | 0.222 |
| | Surface | 0.0 - 2.0 | 1.0 | 0.961 | 0.194 | 0.223 |
| Sept. 27 | Aircraft | 0.0 - 1.0 | 0.4 | 0.862 | | |
| | Aircraft | 1.0 - 2.0 | 0.3 | 0.855 | | |
| | Aircraft | 2.0 - 3.0 | 0.3 | 0.881 | 0.178 | 0.200 |
| | Surface | 0.0 - 3.0 | 1.0 | 0.853 | 0.178 | 0.200 |
| Sept. 29 | Aircraft | 0.0 - 1.5 | 1.0 | 0.839 | 0.183 | 0.202 |
| | Surface | 0.0- 1.5 | 1.0 | 0.867 | 0.183 | 0.203 |
| Aug. 17 | Aircraft | 0.0 - 2.0 | 1.0 | 0.912 | 0.182 | 0.213 |
| | Aircraft(dry) | 0.0 - 2.0 | 1.0 | 0.904 | 0.182 | 0.212 |
| | Upper limit | 0.0 - 2.0 | 1.0 | 0.945 | 0.185 | 0.216 |
| | Lower limit | 0.0 - 2.0 | 1.0 | 0.639 | 0.164 | 0.188 |
| Aug. 18 | Aircraft | 0.0 - 2.0 | 0.5 | 0.906 | | |
| | Aircraft | 2.0 - 3.0 | 0.5 | 0.948 | 0.181 | 0.208 |
| | Aircraft(dry) | 0.0 - 2.0 | 0.5 | 0.882 | | |
| | Aircraft(dry) | 2.0 - 3.0 | 0.5 | 0.935 | 0.180 | 0.207 |
| | Upper limit | 0.0 - 3.0 | 1.0 | 0.926 | 0.181 | 0.208 |
| | Lower limit | 0.0 - 3.0 | 1.0 | 0.675 | 0.170 | 0.192 |
| Aug. 19 | Aircraft | 0.0 - 1.0 | 0.3 | 0.893 | | |
| | Aircraft | 1.0 - 2.0 | 0.7 | 0.954 | 0.184 | 0.216 |
| | Aircraft(dry) | 0.0 - 1.0 | 0.3 | 0.878 | | |
| | Aircraft(dry) | 1.0 - 2.0 | 0.7 | 0.933 | 0.183 | 0.214 |
| | Upper limit | 0.0 - 2.0 | 1.0 | 0.968 | 0.186 | 0.219 |
| | Lower limit | 0.0 - 2.0 | 1.0 | 0.706 | 0.169 | 0.194 |
| Aug. 20 | Aircraft | 0.0 - 1.5 | 0.6 | 0.934 | | |
| | Aircraft | 1.5 - 3.0 | 0.4 | 0.940 | 0.186 | 0.223 |
| | Aircraft(dry) | 0.0 - 1.5 | 0.6 | 0.926 | | |
| | Aircraft(dry) | 1.5 - 3.0 | 0.4 | 0.927 | 0.185 | 0.222 |
| | Upper limit | 0.0 - 3.0 | 1.0 | 0.952 | 0.188 | 0.225 |
| | Lower limit | 0.0 - 3.0 | 1.0 | 0.667 | 0.162 | 0.190 |

The surface albedo is set to 0.2 for the computation. The water vapor profile derived from soundings and from the midlatitude summer profile [*McClatchey et al.*, 1972] is used for the April and September 1997 cases and August 1998 cases, respectively.

14, 1998, we can check the accuracy of the direct irradiance measured by pyrheliometers. Direct irradiances measured by the two pyrheliometers on August 14 agree with those measured by the cavity radiometer within 3 W m$^{-2}$. Since the cavity radiometer is known to be accurate within ±0.3%, these results support that $\tau_{\mathrm{mfrsr}}$ is within a reasonable accuracy. However, the multifilter rotating shadowband radiometer measured the extinction in the direction of the Sun, while the Raman lidar and aircraft measurements sample particles that are not in the same direction. Therefore the agreement of the direct irradiance does not eliminate the problem of sampling if particles are spatially and temporally inhomogeneous.

### 4.2. Sensitivity to the Albedo of the Atmosphere

Given the consistency between $\tau_{\mathrm{p}}$ and $\tau_{\mathrm{mfrsr}}$, on April 14, September 27, and September 29 we are more confident to derive the single-scattering albedo profile on these days than the August 1998 cases. The single-scattering albedo $\varpi$ varies from 0.839 to 0.945 on these 3 days when it is averaged over the vertical layers indicated in Table 3. Since the single-scattering albedo $\varpi$ derived from the surface data is 0.03 to 0.04 different from $\varpi$ derived from aircraft data taken at the lowest altitude, we address the sensitivity of the top of the atmosphere albedo to these differences. When the difference between $\tau_{\mathrm{p}}$ and $\tau_{\mathrm{mfrsr}}$ is larger (the August 1998 cases), we treat the difference as the uncertainty in the single-scattering albedo and perform a sensitivity study of the top of the atmosphere albedo to that uncertainty. The highest $\varpi$ is given by treating the difference between $\tau_{\mathrm{p}}$ and $\tau_{\mathrm{mfrsr}}$ as scattering. The lowest $\varpi$ is given by treating the difference as absorption. However, we believe that the low limit of $\varpi$ is the value derived from dry particles, which is $\varpi$ computed without the humidity correction to the scattering coefficient

measured by the integrating nephelometer. The resulting $\varpi$ varies from 0.878 to 0.968 when it is averaged over the vertical layers indicated in Table 3. In computing the asymmetry parameter, we assume a lognormal number distribution for particles with a mode radius of 0.1 $\mu$m and a geometric standard deviation of 1.4, and we use the refractive index of ammonium sulfate given by *Toon et al.* [1976].

The maximum difference in the top of the atmosphere albedo using $\varpi$ derived from the surface and aircraft data is 0.001. The difference in the top of the atmosphere albedo resulting from the upper and dry particle limits of the single-scattering albedo slightly increases with the solar zenith angle; the maximum difference is 0.003 for the four August cases (Table 3). Since the globally and diurnally averaged downward irradiance at the top of the atmosphere is 342 $\mathrm{W\,m^{-2}}$, the differences in the albedo of 0.001 and 0.003 correspond approximately to 0.3 and 1 $\mathrm{W\,m^{-2}}$ in the irradiance, respectively. Therefore the difference in the top of the atmosphere albedo for these three cases indicates that using the single-scattering albedo measured at the surface instead of using a profile derived from aircraft measurements leads to a smaller perturbation of the upward irradiance at the top of the atmosphere than the estimated global averaged direct aerosol forcing perturbation of -1 $\mathrm{W\,m^{-2}}$ for sulfate aerosols [*Charlson et al.*, 1992]. When the difference between $\tau_{\mathrm{p}}$ and $\tau_{\mathrm{mfrsr}}$ is greater than the uncertainty in $\tau_{\mathrm{mfrsr}}$, the uncertainty in $\varpi$ introduces an equivalent perturbation of the top of the atmosphere albedo to the estimated global averaged direct aerosol forcing perturbation. This sensitivity depends on the size distribution of particles. We assumed a mode radius of a lognormal number distribution of 0.1 $\mu$m and a geometric standard deviation of 1.4. When the size of particles increases, we expect that the top of the atmosphere albedo is less sensitive to $\varpi$ at given extinction optical thickness because of increase of the forward scattering by particles. Nevertheless, this sensitivity analysis illustrates the difficulty in computing the direct aerosol forcing perturbation given the uncertainty in currently available data sets.

## 5. Conclusion

We obtained the ratio of the scattering coefficient measured under wet and dry conditions as a function of relative humidity $f_{\mathrm{sca}}$ from two integrating nephelometers operated under different relative humidity conditions at the surface in order to correct the scattering coefficient measured by an airborne integrating nephelometer. The correction does not significantly increase the scattering coefficient measured under the dry conditions of April 14, September 27, and September 29, indicating that particles present on these days were fairly dry. The differences between the extinction optical thickness of particles $\tau_{\mathrm{p}}$ and the aerosol extinction optical thickness derived from the multifilter rotating shadowband radiometer $\tau_{\mathrm{mfrsr}}$ at 550 nm are 0.01, 0.02, and 0.01 for April 14, September 27, and September 29, respectively; $\tau_{\mathrm{p}}$ is smaller for all three cases. If we take into account the uncertainties of both optical thicknesses, these differences are not significant.

For most of the August 1998 cases, the scattering coefficient profile derived from the airborne integrating nephelometer missed sharp increases in the scattering coefficient at the top of the boundary layer, which are shown in the Raman lidar extinction profile. The value of $\tau_{\mathrm{p}}$ is 72% of $\tau_{\mathrm{mfrsr}}$ when these values are averaged over four flight periods. The difference between the modeled direct irradiance computed using $\tau_{\mathrm{mfrsr}}$ and the measured direct irradiance by pyrheliometers is 1.3%, which supports that $\tau_{\mathrm{mfrsr}}$ is within a reasonable accuracy. Since an impactor was operated upstream of the integrating nephelometer and particle soot absorption photometer to remove particles larger than 1 $\mu$m, missing large particles can be responsible for the difference. Large variations in the extinction coefficient derived from the Raman lidar and in the scattering coefficients measured at the top of the boundary layer indicate a rapid change of the optical properties of particles in these cases. This temporal and spatial variability can contribute to the differences of these extinction optical thicknesses. Furthermore, cloud contamination in $\tau_{\mathrm{mfrsr}}$ and the error in the humidity correction to the integrating nephelometer data can contribute the difference.

Based on the comparison of the extinction optical thickness, the single-scattering albedo for seven cases varies from 0.84 to 0.97. When the difference between the optical thickness of particles derived from aircraft measurements and optical thickness of aerosol derived from the multifilter rotating shadowband radiometer is greater than the instrument uncertainties, the sensitivity of the top of the atmosphere albedo to possible variations in the single-scattering albedo indicates that the uncertainty in the single-scattering albedo gives an equivalent perturbation of the top of the atmosphere albedo to the estimated globally averaged direct aerosol forcing perturbation.

**Acknowledgments.** We thank J. Ogren for useful advice regarding the instruments used for aircraft measurements, P. Daum, J. Hubbe and V. Morris for supplying the aircraft data and for useful discussions regarding the accuracy of the data, and P. Wang for discussion regarding stratospheric aerosol. Data were obtained from the Atmospheric Radiation Measurement (ARM) Program sponsored by the U.S. Department of Energy, Office of Energy Research, Office of Health and Environmental Research, Environmental Sciences Division. One of the authors (S.K.) is supported by the NASA Clouds and the Earth's Radiant Energy System grant NAG-1-1963. Work at Pacific Northwest National Laboratory (PNNL) was supported by DOE under contract DE-ACD6-76RLO 1830. PNNL is operated for DOE by Battelle Memorial Institute. The work at the Pennsylvania State University and State University of New York was supported by Department of Energy Atmospheric Ra-

diation Measurement Program under grant DOE DE-FG02-90ER-61071 and -61702, respectively.

## References

Anderson, T. L., and J. A. Ogren, Determining aerosol radiative properties using the TSI 3563 integrating nephelometer, *Aerosol Sci. Technol., 29,* 57-69, 1998.

Anderson, T. L., et al., Performance characteristics of a high-sensitivity, three-wavelength, total / scatter / backscatter nephelometer, *J. Atmos. Oceanic Technol., 13,* 967-986, 1996.

Ångström, A., On the atmosphere transmission of Sun radiation and on dust in the air, *Geogra. Ann., 11,* 156-166, 1929. also in *Selected Papers on Scattering in the Atmosphere,* SPIE Milestone Ser., vol. M57, edited by C. F. Bohren, The International Society for Optical Engineering, Bellingham, Wash., 1989.

Bergin, M. H., J. A. Ogren, S. E. Schwartz, and L. M. McInnes, Evaporation of ammonium nitrate aerosol in a heated nephelometer: Implication for field measurements, *Environ. Sci. Technol., 31,* 2878-2883, 1997.

Bergin, M. H., S. E. Schwartz, R. N. Halthore, J. A. Ogren, and D. L. Hlavka, Comparison of aerosol optical depth inferred from surface measurements with that determined by Sun photometry for cloud-free conditions at a continental U.S. site, *J. Geophys. Res.,* in press, 2000.

Bond, T. C., T. L. Anderson, and D. Campbell, Calibration and intercomparison of filter-based measurements of visible light absorption by aerosol, *Aerosol Sci. Technol., 30,* 582-600, 1999.

Bohren, C. F., and D. R. Huffman, *Absorption and Scattering of Light by Small Particles,* pp. 132, 172, John Wiley, New York, 1983.

Brasseur, G., and S. Solomon, *Aeronomy of the middle atmosphere, chemistry and physics of the stratosphere and mesosphere,* D. Reidel, Norwell, Mass., 1984.

Charlson, R. J., S. E. Schwartz, J. M. Hales, R. D. Cess, J. A. Coakley Jr., J. E. Hansen, and D. J. Hofmann, Climate forcing by anthropogenic aerosols, *Science, 255,* 423-429, 1992.

Clarke, A. D., J. N. Porter, F. P. J. Valero, and P. Pilewskie, Vertical profiles, aerosol microphysics, and optical closure during the Atlantic Stratocumuls Transition Experiment: Measured and modeled column optical properties, *J. Geophys. Res., 101,* 4443-4453, 1996.

Goldsmith, J. E. M., F. H. Blair, S. E. Bisson, and D. D. Turner, Turn-key Raman lidar for profiling atmospheric water vapor, clouds, and aerosol, *Appl. Opt., 37,* 4979-4990, 1998.

Hänel, G., The properties of atmospheric aerosol particles as function of the relative humidity at thermodynamic equilibrium with the surrounding moist air, *Adv. Geophys., 19,* 74-183, 1976.

Hansen, J. E., and L. D. Travis, Light scattering in planetary atmospheres, *Space Sci. Rev., 16,* 527-610, 1974.

Harrison, L., and J. Michalsky, Objective algorithms for the retrieval of optical depths from ground-based measurements, *Appl. Opt., 22,* 5126-5132, 1994.

Harrison, L., J. Michalsky, and J. Berndt, Automated multifilter rotating shadow-band radiometer: An instrument for optical depth and radiation measurements, *Appl. Opt., 22,* 5118-5125, 1994.

Hegg, D., T. Larson, and P.-O. Yuen, A theoretical study of the effect of relative humidity on light scattering by tropospheric aerosols, *J. Geophys. Res., 98,* 18,435-18,439, 1993.

Hegg, D. A., J. Livingston, P. V. Hobbs, T. Novakov, and P. Russell, Chemical apportionment of aerosol column optical depth off the mid-Atlantic coast of the United States, *J. Geophys. Res., 102,* 25,293-25,303, 1997.

Heintzenberg, J., and R. J. Charlson, Design and application of the integrating nephelometer: a review, *J. Atmos. Oceanic Technol., 13,* 987-1000, 1996.

Holben, B. N., et al., AERONET: A federated instrument network and data archive for aerosol characterization, *Remote Sens. Environ., 66,* 1-16, 1998.

Kato, S., T. P. Ackerman, E. E. Clothiaux, J. H. Mather, G. G. Mace, M. L. Wesely, F. Murcray, and J. Michalsky, Uncertainties in modeled and measured clear-sky surface shortwave irradiances, *J. Geophys. Res., 102,* 25,881-25,898, 1997.

Kato, S., T. P. Ackerman, J. H. Mather, and E. E. Clothiaux, The *k*-distribution method and correlated-*k* approximation for a shortwave radiative transfer model, *J. Quant. Spectrosc. Radiat. Transfer, 62,* 109-121, 1999.

Luke, W. T., R. R. Dickerson, W. F. Ryan, K. E. Pickering, and L. J. Nunnermacker, Tropospheric chemistry over the Lower Great Plains of the United States, 2, Trace gas profiles and distributions, *J. Geophys, Res., 97,* 20,647-20,670, 1992.

McClatchey, R. A., R. W. Fenn, J. E. A. Selby, F. E. Volz, and J. S. Garing, *Optical Properties of the Atmosphere,* 3rd ed., *Environ Res. Pap. 411,* 110 pp., Air Force Cambridge Res. Lab., Bedford, Mass., 1972.

McInnes, L., M. Bergin, and J. Ogren, Apportionment of light scattering and hygroscopic growth to aerosol composition, *Geophys. Res. Lett., 25,* 513-516, 1998.

Ogren, J. A., S. Anthony, J. Barnes, M. H. Bergin, W. Huang, L. M. McInnes, C. Myers, P. Sheridan, S. Thaxton, and J. Wendell, Aerosol and radiation, in *Summary Report 1994-1995,* edited by D.J. Hofmann, J.T. Peterson, and R.M. Rosson, pp. 50-60, Natl. Oceanic and Atmos. Admin. Clim. Monit. Lab. 23, Natl. Oceanic and Atmos. Admin., Boulder, Colo., 1996.

Prospero, J. M., R. J. Charlson, V. Mohnen, R. Jaenicke, A. C. Delany, J. Moyers, W. Zoller, and K. Rahn, The atmospheric aerosol system: An overview, *Rev. Geophys., 21,* 1607-1629, 1983.

Remer, L. A., S. Casseó, D. A. Hegg, Y. J. Kaufman, and B. N. Holben, Urban/industrial aerosol: Ground-based Sun/sky radiometer and airborne in situ measurements, *J. Geophys. Res., 102,* 16,849-16,859, 1997.

Rood, M. J., D. S. Covert, and T. V. Larson, Hygroscopic properties of atmospheric aerosol in Riverside, California, *Tellus, 39B,* 383-397, 1987.

Ryan, W. F., R. R. Dickerson, G. J. Huffman, and W. T. Luke, Tropospheric chemistry over the Lower Great Plains of the United States, 1. Meteorology, *J. Geophys. Res., 97,* 17,963-17,984, 1992.

Schmid, B. J., et al., Clear sky closure studies of lower tropospheric aerosol and water vapor during ACE-2 using airborne sunphotometer, airborne in-situ, space-borne, and ground-based measurements, *Tellus,* in press, 2000.

Shaw, G. E., Sun photometry, *Bull. Am. Meteorol. Soc., 64,* 4-10, 1983.

Sheridan, P. J., and J. A. Ogren, Observations of the vertical and regional variability of aerosol optical properties over central and eastern North America, *J. Geophys. Res., 104,* 16,793-16,805, 1999.

Tang, I. N., and H. R. Munkelwitz, Aerosol phase transformation and growth in the atmosphere, *J. Appl. Meteorol., 33,* 791-796, 1994.

Thomason, L. W., G. S. Kent, C. R. Trepte, and L. R. Poole, A comparison of the stratospheric aerosol background periods of 1979 and 1981-1991, *J. Geophys. Res., 102,* 3611-3616, 1997a.

Thomason, L. W., L. R. Poole, and T. Deshler, A global

climatology of stratospheric aerosol surface area density deduced from Stratospheric Aerosol and Gas Experiment II measurements: 1984-1994, *J. Geophys. Res., 102,* 8967-8976, 1997b.

Toon, B. O., J. B. Pollack, and B. N. Khare, The optical constants of several atmospheric aerosol species: Ammonium sulfate, ammonium oxide, and sodium chloride, *J. Geophys. Res., 81,* 5733-5748, 1976.

Wilks, D. S., *Statistical Methods in the Atmospheric Sciences,* Academic, pp. 159-181, San Diego, Calif., 1995.

T.P. Ackerman, N. Laulainen, and D.D. Turner, P.O. Box 999, Pacific Northwest National Laboratory, Richland, WA 99352-0999.

M.H. Bergin, School of Civil and Environmental Engineering and School of Earth and Atmospheric Science, Georgia Institute of Technology, Atlanta, GA 30332-0512.

T.P. Charlock and R.A. Ferrare, Atmospheric Sciences, Mail Stop 420, NASA Langley Research Center, Hampton, VA 23681-2199.

E.E. Clothiaux, Department of Meteorology, The Pennsylvania State University, 503 Walker Building, University Park, PA 16802.

R.N. Halthore, Department of Applied Science, Brookhaven National Laboratory, Upton, NY 11973-5000.

S. Kato, Atmospheric Sciences, Mail Stop 420, NASA Langley Research Center, Hampton, VA 23681-2199. (s.kato@larc.nasa.gov)

G.G. Mace, Department of Meteorology, University of Utah, 819 Wm. C. Browning Building, Salt Lake City, UT 84112.

J. Michalsky, Atmospheric Sciences Research Center, State University of New York Albany, 251 Fuller Rd., Albany, NY 12205.

(Received July 19, 1999; revised December 1, 1999; accepted December 9, 1999.)